

Determination of gold nanorods concentrations from optoacoustic signals using a three-wavelength hybrid system based on high-power diode lasers and a diode laser bar

Luca LEGGIO*, Sandeep Babu GAWALI, Daniel GALLEGRO, Sergio RODRÍGUEZ, Miguel SÁNCHEZ, Guillermo CARPINTERO and Horacio LAMELA

Department of Electronics Technology, Optoelectronic and Laser Technology Group (GOTL), University Carlos III of Madrid, Av. de la Universidad, 30, 28911 Leganés (Spain) (lleggio@ing.uc3m.es)

Abstract

The main advantage of optoacoustic imaging (OAI) is the capability to detect diseases at their early stages of growth. The efficiency of this technique has been demonstrated by preliminary studies with real biological tissues and small animals. The definitive goal of *in-vivo* OAI is to provide maps of the absolute concentration of chromophores with the help of exogenous optical contrast agents. Usually, solid-state lasers are used for the generation of ultrasounds but their use in clinical environment is inconvenient due to their large sizes, high costs, and low repetition rates (a few Hz) that are not sufficient for a high resolution during image processing. However, the requirements of high repetition rates (up a few kHz) can be fulfilled by high-power diode lasers (HPDLs) combined in side-by-side arrays. In the present paper, we implement a three-wavelength optoacoustic (OA) system consisting on a small array of HPDLs and a diode laser bar (DLB) operating at 870 nm, 905 nm, and 972 nm, respectively, coupled to a 1.2-mm diameter optical fiber bundle. The combined beam illuminates different mixtures of two gold nanorods solutions with absorbance peak at ~ 860 nm and ~ 900 nm, respectively, to generate OA signals. The pulses produced to generate OA signals are alternated between the three wavelengths by a microcontroller circuit with fast switching (0.33 ms). An inverse algorithm is implemented to estimate the concentrations of the nanoparticles solutions from the amplitude of the OA signals. The results achieved with our system show good agreement between the concentrations of gold nanorods estimated from measurements and the expected values.

1. Introduction

Breast cancer is one of the most diffused and differentiated kind of cancer in the world existing in a wide variety of forms [1]. Despite the many efforts for early detection of tumors, there is still inadequate technology for immediate application. The most classical x-ray mammography does not provide an adequate differentiation between benign and malign tumors and the use of ionizing radiation is risky for the health of the patient [2].

Ultrasonic and optical imaging techniques have successfully demonstrated a high specificity in differential diagnosis of malignant and benign tumors and are absolutely harmless to human body [3, 4]. Ultrasonic imaging provides high spatial resolution with high penetration depth, but the contrast between malignant and healthy tissues is not appropriately enough [5]. Optical imaging offers good spatial resolution with high optical contrast, but is limited to a few millimeters in biological tissues [6].

L. LEGGIO, S.B. GAWALI, D. GALLEG0, S. RODRÍGUEZ, M. SÁNCHEZ, et al.
Determination of gold nanorods concentrations from optoacoustic signals ...

In this regard, OAI has been developed as an innovative hybrid imaging modality, since it combines the high spatial resolution and the high penetration depth of ultrasonic imaging with the high optical contrast of optical imaging [7, 8]. It is based on the OA effect that generates pressure waves by a two-steps process. Firstly, a short optical pulse (width of nanoseconds) with high energy illuminates a biological tissue. Considering that the biological tissue is turbid, a portion of the incident light energy is absorbed inside producing heat fluctuations, which result in a thermoelastic expansion of the tissue. Afterwards, the resulting thermoelastic expansion of the tissue generates a pressure wave in the form of an OA signal. The OA signals are then detected by a piezoelectric transducer with a specific bandwidth. The time delay between the generation and the detection of the ultrasonic wave determines the depth of the chromophore detected, as in other imaging techniques. The amplitude of the OA signals depends on the optical absorption coefficient of the biological chromophore under study. This technique can provide 3D images of optical absorption maps in biological tissues in-vivo [9, 10].

In OAI, the most significant aspect is the contrast between the chromophores (i.e. oxy- and deoxy-hemoglobin) and the determination of their optical properties. The lack of contrast between cancer progression at early stages and healthy soft tissues represents the main weakness of the OA techniques for cancer diagnostics, due to their analogous optical properties. The support of contrast agents targeted to specific tissues of human body is necessary to improve the cancer diagnosis [11]. At this purpose, contrast agents based on nanoparticles are potentially beneficial for improving biomedical in-vivo diagnostics and their synthetization has ascended in the biotechnology industry [12, 13]. In particular, the growing interest in the use of nanostructures for biomedical applications has stimulated the

synthesis of gold nanoparticles (GNPs) with tunable size and geometry [14, 15]. The main advantage of GNPs is that their absorption peak can be adjusted to the desired wavelength by changing their geometrical characteristics. Their in-vivo functionality as contrast agents for cancer detection has been demonstrated [16]. Generally, their characteristics allow a preferential accumulation within cancerous tissues instead of healthy tissues. Normally, GNPs with absorption peak close to the emission wavelength of the laser source are chosen in order to improve the OA signal detection and, consequently, to enhance the image contrast. The use of multi-wavelength sources is particularly useful to observe the contrast between the chromophores detected at different wavelengths.

In this regard, pulsed HPDLs are diffusely used for OA generation and are often preferred to solid-state lasers (i.e. Nd:YAG and Ti-Sapphire), due to their higher repetition rates with high energy pulses, lower costs, less cooling requirements, and reasonably smaller and more compact sizes for clinical applications [17-22]. Additionally, HPDLs can be driven with repetition rates up to a few kHz (typically 1 kHz), while Nd:YAG-based systems typically work with 10-30 Hz of repetition rate. A larger repetition rate allows a faster and more efficient image acquisition. Nonetheless, the main challenge of HPDLs is that the pulse energy generated is a few μJ , while the solid-state lasers emit light energy in the order of mJ (but with low repetition rates), required for OA applications in human body. As a solution, a side-by-side combination of many HPDLs can overcome these limitations of optical energy delivered to the tissues. Moreover, the lack of a necessary number of wavelengths in the market represents one of the main drawbacks of HPDLs. In fact, it is required a large number of wavelengths for a functional OA spectroscopy of specific chromophores.

L. LEGGIO, S.B. GAWALI, D. GALLEGO, S. RODRÍGUEZ, M. SÁNCHEZ, et al.
Determination of gold nanorods concentrations from optoacoustic signals ...

In this paper, OA signals are generated from mixed solutions of gold nanorods with absorption peaks at ~ 860 nm and ~ 900 nm by using two small arrays of HPDLs and a DLB operating at 870 nm, 905 nm, and 972 nm, respectively, coupled to a 7-to-1 optical fiber bundle with 1.2-mm diameter. The fiber bundle consists on seven multimode optical fibers with core diameter of 400 μm . A microcontroller circuit generates alternate pulses between the two wavelengths with fast switching of 0.33 ms. The combined beam illuminates some mixtures of two gold nanorods solutions with absorbance peak at ~ 860 nm and ~ 900 nm, respectively, to generate OA signals. The reason of choosing gold nanorods is due to their potential ability as contrast agents in real OAI scenarios, where they can be injected in the body to help the detection of chromophores at specific wavelengths. In this case, it would be particularly useful to know their concentrations in real time.

The purpose of this paper is to estimate the absolute concentrations of the gold nanorods solutions mixed in different proportions (40/60, 50/50, and 60/40) from the analysis of the OA signals detected. The measured OA signals are related to the nanoparticles concentrations by using an inverse algorithm [23] which is based on a fluence model. The use of a third wavelength (972 nm), which is further away from the absorbance peaks of the gold nanorods with respect to the wavelengths of the HPDLs, allows a more precise estimation of their absolute concentrations. Results show very good agreement between estimated and expected values.

The paper is organized as follows: section 2 gives a detailed description of the OA system, section 3 describes the characteristics of the gold nanorods used in the experiments and introduces the inverse algorithm to estimate their concentrations from detected OA signals. Finally, section 4 discusses the results showing the estimation of the single concentrations of gold

nanorods.

2. Measurement setup

In this section we describe the measurement setup used for our experiments. The system is divided into two blocks: the first one includes the laser sources, the optical elements and the electronics, while the second one the measurement setup for the OA signal generation, detection and visualization.

2.1. Laser sources, optical elements and electronics

The excitation system is composed of two triplets of epitaxially-stacked pulsed HPDLs and a DLB combined side-by-side: one triplet with central wavelength at 870 nm (L11348-330-04, Hamamatsu Photonics K.K.) and the other one at 905 nm (SPL PL90_3, OSRAM Opto Semiconductors GmbH), driven individually by diode laser drivers (PCO-7120, IXYS Colorado), while the DLB (SPL BK98-20H, OSRAM Opto Semiconductors GmbH and packaged by DILAS Diodenlaser) operates at 972 nm and is driven by a diode laser driver produced in-house. Table 1 summarizes the characteristics of the HPDLs used in the experiments.

Each laser output is separately coupled into a 400- μm multimode optical fiber (FT400EMT, Thorlabs Inc.) with a numerical aperture (N.A.) of 0.39, as shown in Fig. 1. The optical fibers are joined together forming a fiber bundle built in-house, composed of seven optical fibers disposed in hexagonal configuration and with an output diameter of 1.2-mm, as shown in Fig. 2(a) and (b), where each output is labeled with the corresponding wavelength. In this way, the collective output of the HPDLs results in a higher contribution of optical power. The output optical power will illuminate the sample that in our case is a solution of gold nanorods hosted in a quartz cuvette.

L. LEGGIO, S.B. GAWALI, D. GALLEG0, S. RODRÍGUEZ, M. SÁNCHEZ, et al.
Determination of gold nanorods concentrations from optoacoustic signals ...

Table 1. Characteristics of the light sources used in the experiments. *operates in quasi-continuous wave

| Characteristics | 870-nm HPDL | 905-nm HPDL | 972-nm DLB* |
|-----------------------|---|---|---|
| Peak power (max) | 90 W | 90 W | 215 W |
| Forward current (max) | 35 A | 40 A | 200 A |
| Pulse width (max) | 100 ns | 100 ns | - |
| Duty cycle (max) | 0.075% | 0.1% | - |
| Wavelength (typ.) | 870 nm | 905 nm | 972.3 nm |
| Aperture size | 300 μm \times 10 μm | 200 μm \times 10 μm | 200 μm \times 2 μm (25 emitters, pitch: 400 μm) |
| Divergence angles | 10°, 24° | 9°, 25° | 61.5°, 9.5° |

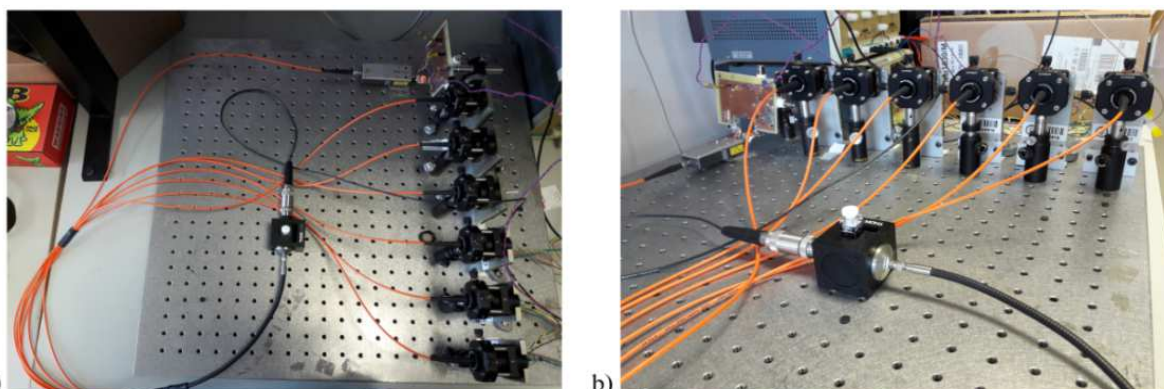


Figure 1. Side-by-side beam coupling of the laser sources into optical fibers. The output of the fiber bundle illuminates a quartz cuvette containing a gold nanorods solution to generate OA signals: a) top view, b) front view.

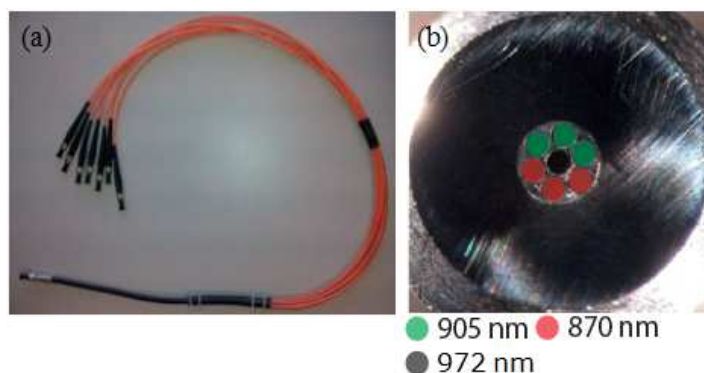


Figure 2. Fiber bundle with 1.2-mm diameter composed of seven 400- μm optical fibers: a) top view of the fiber bundle before being mounted, b) output of the fiber bundle seen under the microscope. The optical fibers are disposed symmetrically between 870 and 905 nm, with the 972 nm output at the center of the bundle to ensure uniform illumination of the sample.

L. LEGGIO, S.B. GAWALI, D. GALLEGO, S. RODRÍGUEZ, M. SÁNCHEZ, et al.
Determination of gold nanorods concentrations from optoacoustic signals ...

The optical pulses emitted by each triplet of HPDLs are perfectly synchronized at the output end of the fiber bundle because they are triggered with the same signal. Individual lens systems formed by a collimating lens (N.A. = 0.40, effective focal length $f_1 = 6.24$ mm) and a focusing lens

(N.A. = 0.68, focal length $f_2 = 3.1$ mm) with anti-reflecting coatings (600-1050 nm) are then used to couple the light emitted by each laser source into 400- μ m multimode optical fibers using a XYZ translation mount to ensure optimum alignment (magnification $M_1 = f_2/f_1 \approx 0.5$).

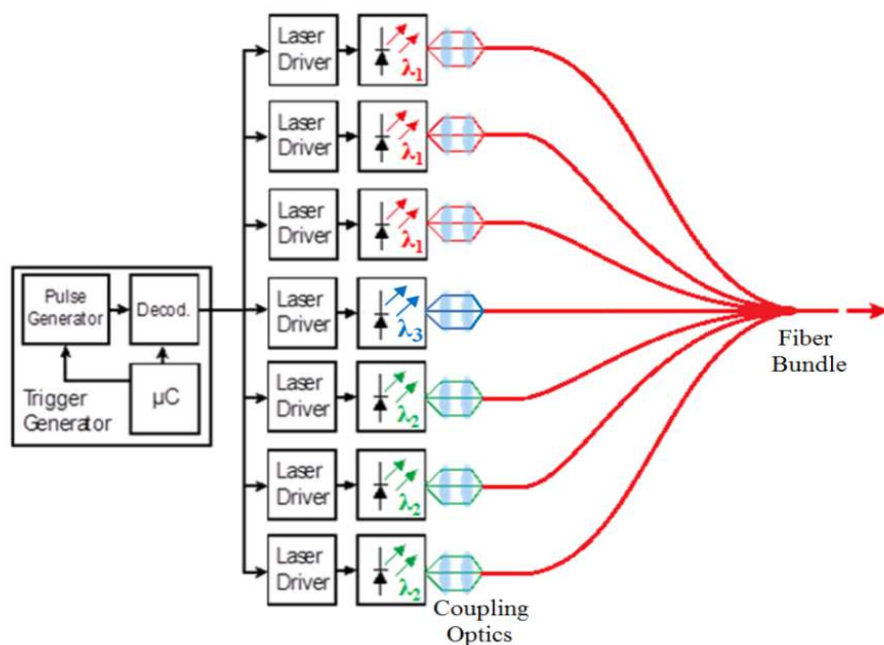


Figure 3. Block diagram of the OA system with light delivery in a fiber bundle.



Figure 4. Microcontroller circuit used to control the pulse emission at the three wavelengths [24].

The emissions of pulses at different wavelengths are time-division multiplexed. Each laser is activated following a proper sequence generated by a trigger generator. This is composed of a microcontroller (μ C), a pulse generator, and a decoder (Fig. 3). The pulses generated are alternated between the three wavelengths by using

a microcontroller circuit able to send separate pulses at each wavelength. The microcontroller circuit (pic32MX250F128B, Microchip Technology Inc., Fig. 4) has been programmed to trigger the pulse generator at some defined periods, T_{WL} , meanwhile it controls the pulse width.

L. LEGGIO, S.B. GAWALI, D. GALLEG0, S. RODRÍGUEZ, M. SÁNCHEZ, et al.
Determination of gold nanorods concentrations from optoacoustic signals ...

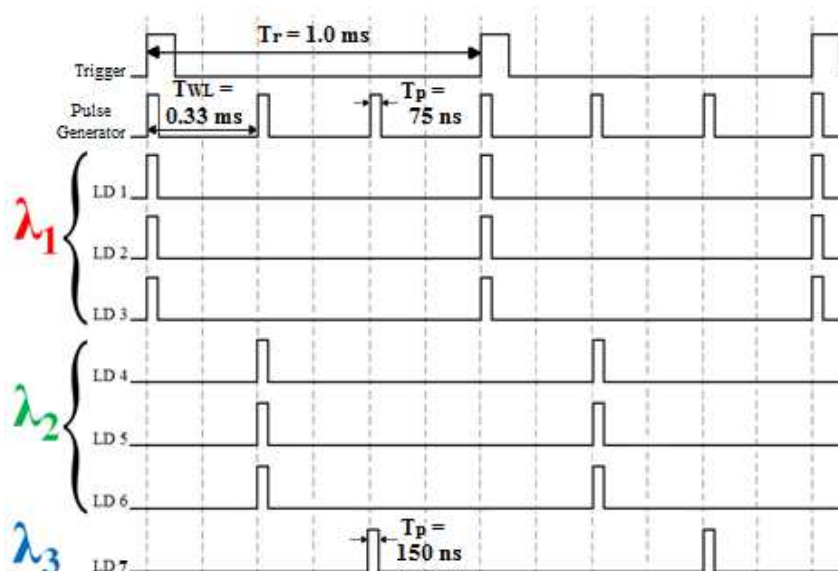


Figure 5. Time diagram that shows how the pulses are alternated between the three wavelengths λ_1 , λ_2 and λ_3 .

Through the decoder the pulse is distributed to the laser drivers up to seven drivers following a flexible programmed sequence that can be adapted to different configurations (Fig. 5). The repetition period T_{WL} corresponds to the switching time between the wavelengths. The HPDLs with the same emission wavelength are activated at the same time. The minimum period between wavelengths is limited by the extinction of the acoustic wave to avoid overlapping. The period of the cycle over all wavelengths, T_R , should be equal or larger than the number of wavelengths, N , times the repetition period T_{WL} ($T_R \geq N * T_{WL}$). Additionally, it cannot be lower than the minimum repetition period of the lasers that depends on the duty cycle (D) and the pulse width T_P . In our implementation we set a repetition period of $T_R = 1.0$ ms (repetition rate of 1 kHz) and a pulse width T_P of 75 ns ($D = 0.0075\%$) for the HPDLs and 150 ns ($D = 0.015\%$) for the DLB, and a T_{WL} of 0.33 ms, which corresponds to the switching time between the three wavelengths. Such a fast switching time would permit a fast image acquisition in a real OAI

application. In our experiments, we switch the times between the three wavelengths for a fast estimation of the concentrations of the gold nanorods solutions.

2.2. Measurement setup for OA signal generation

The measurement setup consists of the fiber bundle output, a cuvette holder containing a 1 cm quartz cuvette (model Z600768-1EA, Hellma GmbH) with path length of 0.4 cm, a 10-MHz piezoelectric transducer (V327-SU, Olympus Corp.), a 40-dB preamplifier, an oscilloscope, and a PC to record the OA signals (Fig. 6). The cuvette holder has four ports in total, including a SMA-fiber-adapter input that has a collimator lens and a port to accommodate the piezoelectric transducer. The OA signals generated are detected by the piezoelectric transducer and then pre-amplified of 40 dB. Afterwards, they are digitized on the oscilloscope, which is synchronized with the pulse emission through the trigger generator.

L. LEGGIO, S.B. GAWALI, D. GALLEGRO, S. RODRÍGUEZ, M. SÁNCHEZ, et al.
Determination of gold nanorods concentrations from optoacoustic signals ...

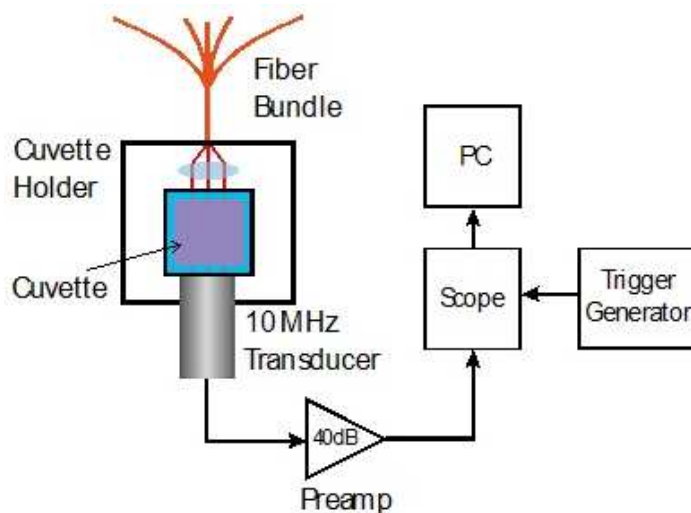


Figure 6. Measurement setup for the detection of OA signals.

Table 2. Characteristics of the optical pulses used for generating the OA signals.

| Parameter | 870-nm HPDLs | 905-nm HPDLs | 972-nm DLB |
|---------------------|--------------|--------------|--------------|
| Pulse width | 75 ns | 75 ns | 150 ns |
| Repetition rate | 1 kHz | 1 kHz | 1 kHz |
| Duty cycle | 0.0075% | 0.0075% | 0.015% |
| Total pulse energy | ~ 16 μ J | ~ 16 μ J | ~ 16 μ J |
| Total average power | ~ 16 mW | ~ 16 mW | ~ 16 mW |

Finally, the OA signals are sent to a PC for recording and filtering. Assuming rectangular pulses with pulse width of 75 ns for the HPDLs and 150 ns for the DLB, and repetition rate of 1 kHz, the total pulse energies provided to the gold nanorods solutions chosen as samples are ~16 μ J at each wavelength. Then, the output of the fiber bundle is collimated by an aspheric lens (N.A. =0.22, focal length $f=12$ mm) with anti-reflection coating (600-1050 nm) to illuminate the sample uniformly. Distilled water is used as a coupling medium between transducer and the wall of the cuvette. The average power measured at the output of the 12 mm lens is ~16 mW at each wavelength. Table 2 reports the characteristics of the optical pulses used for excitation of OA signals at 870, 905, and 972

nm, respectively.

3. Characterization of gold nanorods and inverse algorithm

Gold nanoparticles are considered as a potential contrast agent for discrimination of cancer and other diseases in OA spectroscopy [25]. The most significant features of the gold nanoparticles that affect their optical properties are the position and the amplitude of the absorption peaks in the spectrum that depends on their geometrical characteristics (i.e. length and width).

In this section we describe the characteristics of the gold nanorods solutions and the algorithm for the determination of their absolute concentrations

L. LEGGIO, S.B. GAWALI, D. GALLEGO, S. RODRÍGUEZ, M. SÁNCHEZ, et al.
Determination of gold nanorods concentrations from optoacoustic signals ...

from the OA signals detected. We characterized the absorbance spectrum of two pure solutions of gold nanorods with absorbance peak (optical density (O.D.) = 20) at ~ 860 and ~ 900 nm, respectively, over the spectral range between 410 and 1100 nm (Fig. 7) by using a spectrophotometer (Lambda 14P, Perkin Elmer Inc.) and considering a path length of 1 cm in a quartz cuvette. The main characteristics of the gold nanorods are reported in Table 3. We call NP1 the gold nanorods with absorbance peak at ~ 860 nm,

and NP2 the gold nanorods with absorbance peak at ~ 900 nm. The corresponding absorption coefficients at 870, 905, and 972 nm, reported in Table 4, have been calculated from the measured spectra (Fig. 7) using the following equation [25]:

$$\mu_{abs} \left[\text{cm}^{-1} \right] = 2.303 \times \text{O.D.} \quad (1)$$

considering that O.D. corresponds to the absorbance using a path length of 1cm.

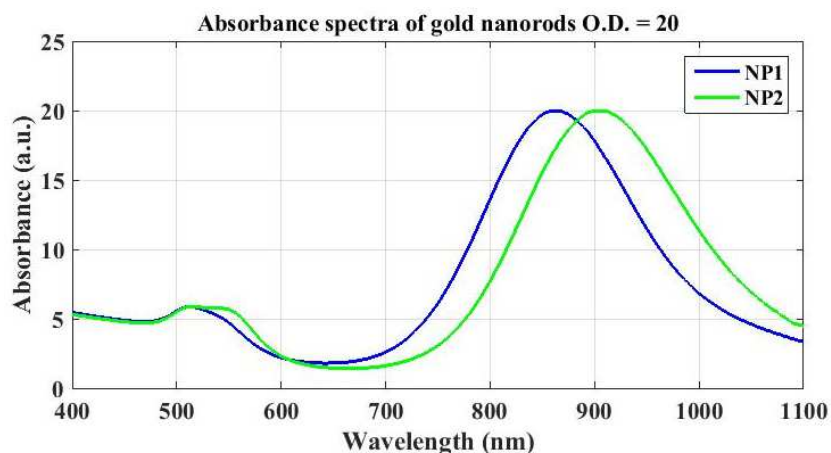


Figure 7. Absorbance spectra of two colloidal solutions of gold nanorods with peak at: ~ 860 nm (blue) and ~ 900 nm (green) (O.D. = 20). The solutions have been diluted with a factor of 20 before measurements.

Table 3. Main characteristics of the gold nanorods.

| Characteristics | NP1 | NP2 |
|-------------------------|-------------------------------|-------------------------------|
| Width | 10.8 ± 0.9 nm | 11.7 ± 0.8 nm |
| Length | 49.6 ± 3.2 nm | 56.3 ± 4.2 nm |
| Aspect ratio | 4.6 | 4.8 |
| Longitudinal peak | 858 nm | 900 nm |
| Transverse peak | 513 nm | 516 nm |
| Particle concentration | 1.3 x 10 ¹³ per ml | 9.9 x 10 ¹³ per ml |
| Mass concentration (Au) | 0.9 mg/ml | 0.8 mg/ml |

L. LEGGIO, S.B. GAWALI, D. GALLEG0, S. RODRÍGUEZ, M. SÁNCHEZ, et al.
Determination of gold nanorods concentrations from optoacoustic signals ...

Table 4. Absorption coefficients of the gold nanorods at 870, 905, and 972 nm.

| Wavelength | Absorption coefficient (cm ⁻¹) | |
|------------|--|--------|
| | NP1 | NP2 |
| 870 nm | ~ 45.8 | ~ 41.7 |
| 905 nm | ~ 39.6 | ~ 46.0 |
| 972 nm | ~ 20.8 | ~ 33.7 |

In previous work [26], an inverse algorithm has been proposed to estimate optoacoustically the absolute concentrations C_m of M solutions of nanoparticles with known absorption coefficient spectra. The same article states that, considering a set of N operating wavelengths, the total absorption coefficient $\mu_{TOT}(\lambda_n)$ (cm⁻¹) of the mixed solution is a function of the wavelength λ_n and can be expressed as:

$$\mu_{TOT}(\lambda_n) = \sum_{m=1}^M \mu_m(\lambda_n) C_m \quad (2)$$

where $\mu_m(\lambda_n)$ is the known (from the spectra) absorption coefficient (cm⁻¹) of the reference solution of nanoparticles m at wavelength λ_n . After some mathematical steps that we do not report for simplicity, we obtained an $N \times M$ matrix that relates the normalized OA signal amplitudes $B(\lambda_n)$, obtained from the nanoparticles mixtures, with the absorption coefficients multiplied by the single nanoparticles concentrations:

$$\begin{pmatrix} B(\lambda_1) \\ B(\lambda_2) \\ \vdots \\ B(\lambda_N) \end{pmatrix} = k' \begin{bmatrix} \mu_1(\lambda_1) & \cdots & \mu_M(\lambda_1) \\ \vdots & \ddots & \vdots \\ \mu_1(\lambda_N) & \cdots & \mu_M(\lambda_N) \end{bmatrix} \begin{pmatrix} C_1 \\ C_2 \\ \vdots \\ C_M \end{pmatrix} \quad (3)$$

In Eq. (3), $B(\lambda_n) = V(\lambda_n)/(P(\lambda_n)e^{-\mu_{att}(\lambda_n)d})$, where $V(\lambda_n)$ is the peak-to-peak OA signal amplitude, $P(\lambda_n)$ is the average power at the input of the cuvette, and $e^{-\mu_{att}(\lambda_n)d}$ is the exponential

attenuation than depends on the wavelength-dependent attenuation coefficient $\mu_{att}(\lambda_n)$ and light path d inside the cuvette. The parameter $k' = T_R \cdot \Gamma$ is a proportionality term depending on the Grüneisen coefficient Γ (~ 0.1 for aqueous solutions [28]) and the pulse repetition period T_R . The terms $B(\lambda_n)$ can be simplified considering just the signal amplitude that comes from the entrance of the cuvette, which means considering $d \ll 1$. In this case, $e^{-\mu_{att}(\lambda_n)d} \approx 1$ and the system (3) becomes linear. The concentrations C_m can easily found inverting the matrix of absorption coefficients.

4. Results

In our specific case we want to estimate the concentrations C_1 and C_2 of two solutions of gold nanorods (NP1 and NP2) mixed in a quartz cuvette from the evaluation of the OA signals detected at 870 nm, 905 nm, and 972 nm. As anticipated in the introduction, we consider three different mixtures of gold nanorods containing different percentages of the two solutions: I) 40 % NP1 and 60 % NP2, II) 50 % NP1 and 50 % NP2, III) 60 % NP1 and 40 % NP2. For the case of two different absorbers and three wavelengths, Eq. (3) reduces to:

$$\begin{cases} B(\lambda_1) = (\mu_1(\lambda_1) \cdot S_1 + \mu_2(\lambda_1) \cdot S_2) \\ B(\lambda_2) = (\mu_1(\lambda_2) \cdot S_1 + \mu_2(\lambda_2) \cdot S_2) \\ B(\lambda_3) = (\mu_1(\lambda_3) \cdot S_1 + \mu_2(\lambda_3) \cdot S_2) \end{cases} \quad (4)$$

L. LEGGIO, S.B. GAWALI, D. GALLEG0, S. RODRÍGUEZ, M. SÁNCHEZ, et al.
Determination of gold nanorods concentrations from optoacoustic signals ...

where $S_m = k' C_m$, $\lambda_1 = 870 \text{ nm}$, $\lambda_2 = 905 \text{ nm}$ and $\lambda_3 = 972 \text{ nm}$. Solving the linear system of Eq. (4), we find the parameters S_1 and S_2 dependent on the unknown factor k' .

We can express the values of S_1 and S_2 by using the following equations:

$$S_1 = A_1 + A_2 \quad (5)$$

$$S_2 = A_3 + A_4 \quad (6)$$

where the values of A_1 , A_2 , A_3 , and A_4 are expressed by the following equations, respectively:

$$A_1 = \frac{B(\lambda_3)}{k' \mu_1(\lambda_3)} \quad (7)$$

$$A_2 = \frac{\mu_2(\lambda_3)(B(\lambda_2)\mu_1(\lambda_1) - B(\lambda_1)\mu_1(\lambda_2))}{k' \mu_1(\lambda_3)(\mu_1(\lambda_2)\mu_2(\lambda_1) - \mu_1(\lambda_1)\mu_2(\lambda_2))} \quad (8)$$

$$A_3 = \frac{B(\lambda_3)}{k' \mu_2(\lambda_3)} \quad (9)$$

$$A_4 = \frac{\mu_1(\lambda_3)(B(\lambda_2)\mu_2(\lambda_1) - B(\lambda_1)\mu_2(\lambda_2))}{k' \mu_2(\lambda_3)(\mu_1(\lambda_1)\mu_2(\lambda_2) - \mu_1(\lambda_2)\mu_2(\lambda_1))} \quad (10)$$

Finally, the concentrations can be obtained as a volume percent, knowing that the sample is a mixture exclusively of the two solutions of gold nanorods, as follows:

$$C_n(\%) = \frac{S_n}{S_1 + S_2} \times 100 \quad (11)$$

The OA signals detected at 870 nm, 905 nm and 972 nm corresponding to each of the three mixtures are depicted in Fig. 8 (one capture) and their peak-to-peak amplitudes (mean values and standard deviations) are reported in Table 5 after averaging on 10 measurements and boxcar filtering in Matlab.

The single concentrations C_1 and C_2 of the gold nanorods are estimated from the OA signals (Table 6) and are shown to be in good agreement with the expected values. The maximum divergence from the expected value is 1.34 %, which represents a very good result.

Table 5. OA signals at 870, 905 and 972 nm after boxcar filtering in Matlab.

| Wavelength | Optoacoustic signal (mV) | | |
|------------|--------------------------|--------------------|--------------------|
| | 40% NP1 60% NP2 | 50% NP1 50% NP2 | 60% NP1 40% NP2 |
| 870 nm | 56.3 ± 0.1 | 56.5 ± 0.1 | 57.1 ± 0.1 |
| 905 nm | 56.2 ± 0.1 | 55.4 ± 0.1 | 54.6 ± 0.1 |
| 972 nm | 35.8 ± 0.1 | 39.0 ± 0.1 | 42.3 ± 0.1 |

Table 6. Values of the gold nanorods concentrations estimated from the OA signals measured.

| Nanoparticles | Estimated concentrations (%) | | | |
|---------------|------------------------------|--------------------|--------------------|--|
| | 40% NP1 60% NP2 | 50% NP1 50% NP2 | 60% NP1 40% NP2 | |
| C_1 : NP1 | 40.48 | 51.34 | 60.20 | |
| C_2 : NP2 | 59.52 | 48.66 | 39.80 | |
| | ± 1.11 | ± 0.78 | ± 0.58 | |

L. LEGGIO, S.B. GAWALI, D. GALLEGO, S. RODRÍGUEZ, M. SÁNCHEZ, et al.
Determination of gold nanorods concentrations from optoacoustic signals ...

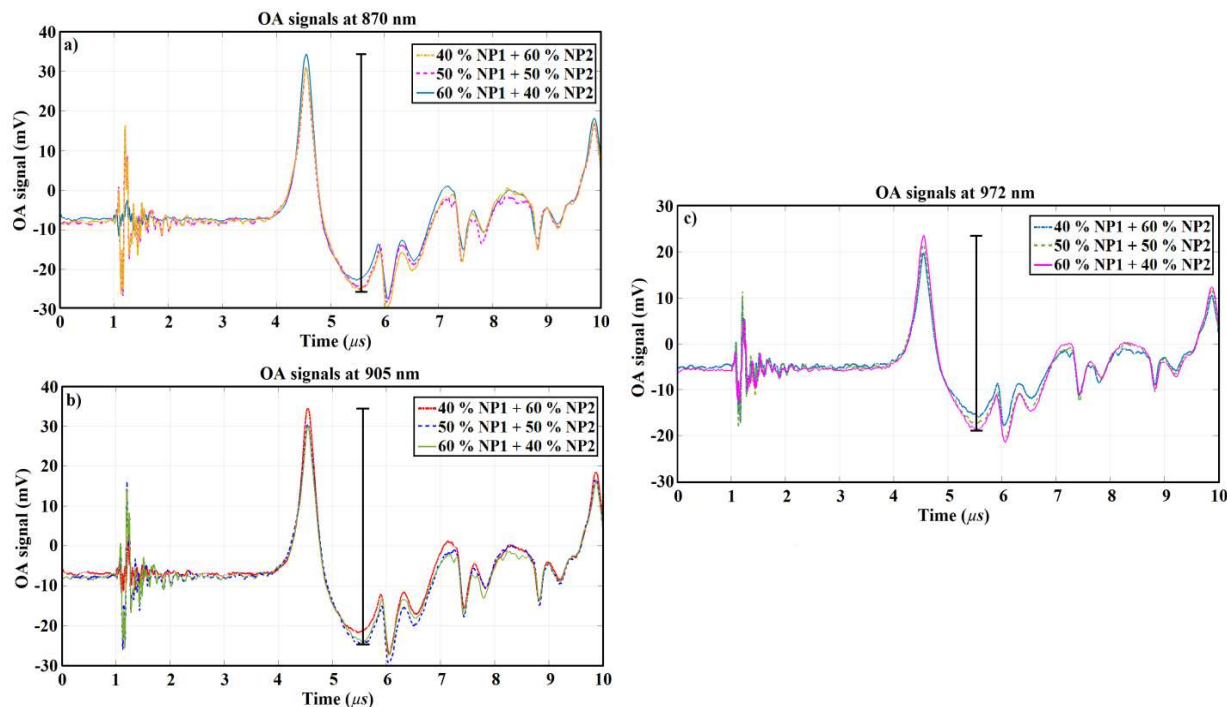


Figure 8. OA signals detected from three different mixtures of gold nanorods at: a) 870, b) 905, and c) 972nm. For the calculation of the concentrations of gold nanorods we considered their peak-to-peak amplitudes.

5. Conclusions

The concentrations of some gold nanorods solutions have been estimated from the amplitudes of the OA signals detected at 870 nm, 905 nm, and 972 nm with the use of HPDLs and a DLB. The results are shown to be in very good agreement with the expected values with acceptable margins of error. The gold nanorods discussed in this paper are considered as potential contrast agents for real OA imaging applications where a differentiation between tissues is necessary to detect the onset of diseases, due to their high absorbance and biocompatibility. This step is also important to estimate the spectral contrast between the chromophores in a biological tissue, organ or specific group of molecules. Future research on this field should be dedicated to add new

wavelengths to the OA system (such as 808 and 940 nm) for potential applications in multi-spectral OA imaging. Actually, working in a larger range of wavelengths would allow a better differentiation between chromophores during the image processing.

Acknowledgment

Our work is supported by EU research project OILTEBIA (Optical Imaging and Laser Techniques for Biomedical Applications).

Declaration of interest

The authors have no financial interests in the manuscript. There are no potential conflicts of interest to declare.

L. LEGGIO, S.B. GAWALI, D. GALLEGRO, S. RODRÍGUEZ, M. SÁNCHEZ, et al.
Determination of gold nanorods concentrations from optoacoustic signals ...

References

- [1] Sun K., Chen X., Chai W., Fei X., Fu C., *et al.* Breast cancer: diffusion Kurtosis MR imaging-diagnostic accuracy and correlation with Clinical-pathologic factors. *RSNA Radiology* 2015;277(1), 46-55.
- [2] Raftery J. and Chorozoglou M. Possible net harms of breast cancer screening: updated modelling of Forrest report. *British Dental Journal* 2012; 212(129); 8 pages.
- [3] Wells P.N.T. Ultrasonic imaging of the human body. *Reports on Progress in Physics* 1999; 62 (5); 671–722.
- [4] Leff D.R., Warren O.J., Enfield L.C., Gibson A., Athanasiou T., *et al.* Diffuse optical imaging of the healthy and diseased breast: a systematic review. *Breast Cancer Research and Treatment* 2008; 108 (1); 9-22.
- [5] Herment A., Guglielmi J.P., Dumeé P., Peronneau P., and Delouche P. Limitations of ultrasound imaging and image restoration. *Ultrasonics* 1987; 25 (5); 267-73.
- [6] Kozacki T., Kujawińska M., and Książewski P. Investigation of limitations of optical diffraction tomography. *Opto-Electronics Review* 2007; 15 (2); 102-109.
- [7] Wang L.V. Multiscale photoacoustic microscopy and computed tomography. *Nature Photonics* 2009; 3; 503–509.
- [8] Lutzweiler C. and Razansky D. Optoacoustic Imaging and Tomography: Reconstruction Approaches and Outstanding Challenges in Image Performance and Quantification. *Sensors* 2013; 13 (6); 7345-7384.
- [9] Mallidi S., Luke G.P., and Emelianov S. Photoacoustic imaging in cancer detection, diagnosis, and treatment guidance. *Trends in Biotechnology* 2011; 29 (5); 213–221.
- [10] Mehrmohammadi M., Yoon S.J., Yeager D., and Emelianov S. Photoacoustic imaging for cancer detection and staging. *Current Molecular Imaging* 2013; 2 (1); 89–105.
- [11] Weber J., Beard P.C., and Bohndiek S.E. Contrast agents for molecular photoacoustic imaging. *Nature Methods* 2016; 13; 639–650.
- [12] Hahn M.A., Singh A.K., Sharma P., Brown S.C., and Moudgil B.M. Nanoparticles as contrast agents for in-vivo bioimaging: current status and future perspectives. *Analytical and Bioanalytical Chemistry* 2011; 399 (1); 3-27.
- [13] Lamela H., Cunningham V., Pedreira P., Gallego D.C., Acedo P., *et al.* Comparative analysis of optical absorption and optoacoustic signal generation in nanoparticles. *Proc. of SPIE* 2008; 6856, 68560L.
- [14] Li W. and Chen X. Gold nanoparticles for photoacoustic imaging. *Nanomedicine* 2015; 10 (2), pp. 299-320.
- [15] Cunningham V., Lamela H., and Gallego D.C. Laser optoacoustic scheme for highly accurate characterization of gold nanostructures in liquid phantoms for biomedical applications. *Journal of Nanophotonics* 2013; 7 (1); 073078.
- [16] Zhang Q., Iwakuma N., Sharma P., Moudgil B.M., Wu C., *et al.* Gold nanoparticles as a contrast agent for in vivo tumor imaging with photoacoustic tomography. *Nanotechnology* 2009; 20 (39); 395102.
- [17] Cunningham V. and Lamela H. Efficient combination of multiple high power semiconductor laser sources for photoacoustic signal generation in biomedical phantoms. *Proc. of SPIE* 2006; 6191; 619106.
- [18] Allen T.J. and Beard P.C. Pulsed near-infrared laser diode excitation system for biomedical photoacoustic imaging. *Optics Letters* 2006; 31 (23); 3462-3464.
- [19] Friedrich C.S., Wawreczko M.C., Mienkina M.P., Gerhardt N.C., Schmitz G., and Hofmann M.R. Compact semiconductor laser sources for photoacoustic imaging. *Proc. of SPIE* 2009; 7177; 71772H.
- [20] Zeng L.M., Liu G.D., Yang D.W., and Ji X.R. Portable optical-resolution photoacoustic microscopy with a pulsed laser diode excitation.

L. LEGGIO, S.B. GAWALI, D. GALLEGRO, S. RODRÍGUEZ, M. SÁNCHEZ, et al.
Determination of gold nanorods concentrations from optoacoustic signals ...

- Appl. Phys. Lett. 2013; 102 (5), 053704.
- [21] Wang T.H., Nandy S., Salehi H.S., Kumavor P.D., and Zhu Q. A low-cost photoacoustic microscopy system with a laser diode excitation. Biomed. Opt. Express 2014; 5 (9); 3053-3058.
- [22] Upputuri P.K. and Pramanik M. Performance characterization of low-cost, high-speed, portable pulsed laser diode photoacoustic tomography (PLD-PAT) system. Biomedical Optics Express 2015; 6 (10); 4118-4129.
- [23] Cox B., Laufer J.G., Arridge S.R., and Beard P.C. Quantitative spectroscopic photoacoustic imaging: a review. Journal of Biomedical Optics 2012; 17 (6); 061202.
- [24] <http://www.microchip.com>
- [25] Li W. and Chen X. Gold nanoparticles for photoacoustic imaging. Nanomedicine 2015; 10 (2); 299-320.
- [26] Leggio L., Gallego D., Arroyo R., Gawali S.B., Rodríguez S., Sánchez M., et al. Accurate determination of gold nanorods concentrations from optoacoustic signals detected at 870 nm and 905 nm by using high-power diode lasers with fast switching electronics. Progress In Electromagnetic Research B 2017;78;143-154.